



1 **Oblique rifting at oceanic ridges:**
2 **Relationship between spreading and stretching directions**
3 **from earthquake focal mechanisms**

4 Marc Fournier, Carole Petit

5
6 CNRS UMR 7072, Laboratoire de Tectonique, Université Pierre et Marie Curie-Paris6, Case
7 129, 4 place Jussieu, 75252 Paris Cedex 05, France

8 marc.fournier@lgs.jussieu.fr Fax: (33) 1-44-27-50-85

9
10 **Abstract.** The relationship between spreading and stretching directions is investigated at
11 oblique-spreading oceanic ridges using earthquake focal mechanisms. The stretching direction
12 at ridge axes corresponds to the direction of the greatest principal strain ϵ_1 taken as the mean
13 trend of the seismic T-axes of extensional earthquake focal mechanisms. It is compared with
14 the spreading direction provided by global plate-motion models. We find that the stretching
15 direction trends approximately halfway between the spreading direction and the normal to the
16 ridge trend, a result in line with analogue experiments of oblique rifting. This result is
17 satisfactorily accounted for with an analytical model of oblique rifting, for which the direction
18 of ϵ_1 is calculated with respect to rifting obliquity for different amounts of stretching using
19 continuum mechanics. For low stretching factors, typical of incremental seismic
20 deformations, ϵ_1 obliquity is two times lower than rifting obliquity. For higher stretching
21 factors, the stretching and spreading directions become parallel.

22
23 **Keywords:** oblique rifting, oblique-spreading ridges, stretching, extension

24 1. Introduction

25 Determining the direction of relative motion between two rigid plates on either side of a
26 deformation zone can be achieved by analysing the strain within the deformation zone. In
27 oblique deformation settings, i.e., when the direction of displacement between the two rigid
28 plates is oblique to the deformation zone, the direction of relative motion is generally not
29 parallel to the principal strain directions (e.g., Sanderson and Marchini, 1984; Tikoff and
30 Teyssier, 1994; Dewey et al., 1998; Fossen and Tikoff, 1998). This result is for example the
31 case at the axial rifts of oblique-spreading mid-oceanic ridges (Taylor et al., 1994; Tuckwell
32 et al., 1996), which are investigated in this paper.

33 The process of oblique divergence between two tectonic plates often involves the
34 formation of an oblique rift. Oblique rifting occurs in the continental domain (e.g. Lake
35 Baikal; Petit et al, 1996) as well as in the oceanic domain at the axis of slow-spreading ridges
36 (e.g., Southwest Indian Ridge). The faulting and strain patterns associated with oblique rifting
37 have been investigated for both oceanic and continental rifts (Dauteuil and Brun, 1993, 1996;
38 Murton and Parson, 1993; Shaw and Lin, 1993; Taylor et al., 1994; Applegate and Shor,
39 1994; Carbotte and Mac Donald, 1994; McAllister et al., 1995; Dauteuil et al., 2001; Acocella
40 and Korme, 2002; Clifton and Schlische, 2003; Fournier et al., 2004a), and by means of
41 experimental (Withjack and Jamison, 1986, Tron and Brun, 1991; Dauteuil and Brun, 1993;
42 McClay and White, 1995; Bonini et al., 1997; Clifton et al., 2000; Mart and Dauteuil, 2000;
43 Clifton and Schlische, 2001; Venkat-Ramani and Tikoff, 2002), analytical (Elliot, 1972;
44 Sanderson and Marchini, 1984; McCoss, 1986; Withjack and Jamison, 1986; Fossen and
45 Tikoff, 1993; Tikoff and Fossen, 1993, 1998; Krantz, 1995; Tuckwell et al., 1996; Abelson
46 and Agnon, 1997), and numerical (Tuckwell et al., 1998) models. These studies show that
47 oblique rifting is accommodated by both normal and strike-slip faults, whose relative
48 proportions and orientations depend on rifting obliquity defined as the angle between the
49 normal to the rift trend and the direction of displacement. Oblique rifting typically produces
50 en echelon fault patterns that are not perpendicular to the direction of relative motion.

51 Withjack and Jamison (1986) demonstrated, with analogue clay models marked at their
52 surface by deformed circles, that three structural directions are linked in the process of
53 oblique rifting: the rift trend (or its perpendicular), the direction of relative motion between
54 the two plates, and the trend of the greatest principal strain axis ϵ_1 of the finite strain ellipsoid
55 (Figure 1). When the direction of relative motion is perpendicular to the rift trend, the rift
56 formation involves pure shear extension without simple shear and the deformation is
57 accommodated by dip-slip normal faults parallel to the rift. The ϵ_1 axis is then horizontal,
58 perpendicular to the normal faults, and parallel to the direction of divergence. When the
59 relative motion is oblique to the rift trend, i.e., in transtensional settings, the rift formation
60 involves a combination of pure shear extension and simple shear. The deformation is
61 accommodated by a combination of normal faults parallel and oblique to the rift trend, and
62 also by strike-slip faults when the rifting obliquity increases. In this case, ϵ_1 is approximately
63 bisector of the angle between the displacement vector and the normal to the rift (Withjack and
64 Jamison, 1986). The analytical solution to the problem of oblique rifting, based on the general
65 theory of transpression-transtension developed by Sanderson and Marchini (1984) and Tikoff
66 and Teyssier (1994), confirms that the infinitesimal extension direction is exactly the bisector
67 of the angle between the displacement vector and the normal to the rift (see also McCoss,
68 1986).

69 Tron and Brun (1991) and Clifton et al. (2000) showed with laboratory experiments that
70 the fault strike distribution in oblique rifts depended on the rifting obliquity. Consequently, a
71 statistical analysis of fault strikes in natural rifts may provide an accurate estimate of the
72 direction of divergence. This rule has been applied successfully to determine the direction of
73 spreading along two slow-spreading ridges, the Mohns Ridge in the North Atlantic Ocean
74 (Dauteuil and Brun, 1993) and the West Sheba Ridge in the Gulf of Aden (Dauteuil et al.,
75 2001), and the kinematic evolution of the Okinawa Trough (Sibuet et al., 1995, Fournier et
76 al., 2001a). Taylor et al. (1994) and Tuckwell et al. (1996) examined the relationship between
77 the orientation of extensional fractures and the plate motion vector at oblique spreading ridges
78 and at so-called “extensional transform zones” (ETZ) characterized by an obliquity between

79 45° and 75° (Taylor et al., 1994). They observed that, at oblique spreading ridges, most
80 normal faults form at an angle with the ridge axis approximately equal to the half of the plate
81 motion obliquity, a result in line with the experiments of Withjack and Jamison (1986), Tron
82 and Brun (1991), and Clifton et al. (2000).

83 However, with the exception of the work of Withjack and Jamison (1986), these studies
84 mainly focused on fault strikes and did not regard the implications in terms of strain. In
85 experimental models as well as in the offshore domain, statistical analysis of fault
86 distributions does not allow estimation of strain axes directions because slip vectors on fault
87 planes cannot be directly observed. In seismically active rifts, however, the direction of
88 maximum stretching can be inferred from earthquake focal mechanisms. In the following, we
89 investigate the relationship between spreading and stretching directions as determined from
90 earthquake focal mechanisms at six oblique spreading ridges.

91

92 **2. Stretching direction determined from earthquake focal mechanisms**

93 In a homogeneous and isotropic material, rupture occurs on two conjugate planes of
94 maximum shear stress oriented with respect to the maximum and minimum stresses σ_1 and σ_3 .
95 Because most earthquakes occur on pre-existing faults, earthquakes do not provide direct
96 evidence for the orientation of principal stresses, but instead provide evidence for the
97 orientation of the strain axes (e.g., Twiss and Unruh, 1998). The compression (P) and tension
98 (T) axes of the double-couple focal mechanism solutions are defined kinematically by fault
99 slip and correspond to the principal strain axes ϵ_3 and ϵ_1 , respectively. They represent the
100 principal axes of the incremental (or instantaneous) strain tensor for fault movements (e.g.,
101 McKenzie, 1969; Marrett and Allmendinger, 1990). Thus, in extensional settings, T-axes of
102 normal faulting earthquakes can be used to determine the direction of stretching. This method
103 is applicable in regions of homogeneous deformation, i.e. when focal mechanisms are all of
104 the same type, which is the case at spreading centres of oceanic ridges.

105

106 **3. Stretching vs spreading directions at oblique spreading ridges**

107 In the oceanic domain, rifting occurs at the crest of slow-spreading mid-oceanic ridges
108 characterised by high seismic activity. Fast spreading centres are devoid of an axial rift and
109 seismicity, and are characterized by orthogonal spreading except in a few back-arc basins
110 where ETZ have been described, such as the Manus and Lau basins (Taylor et al., 1994). At
111 fast spreading ridges, the obliquity between the spreading direction and the plate boundary is
112 taken up by transform faults (e.g., Pacific-Antarctic Ridge). The main oblique-spreading
113 ridges on Earth are the Southwest Indian Ridge (SWIR) in the Indian Ocean (Figure 2; Ewing
114 and Heezen, 1960; Fisher and Sclater, 1983; Patriat, 1987), the Sheba Ridge in the Gulf of
115 Aden (Figure 3; Matthews et al., 1967; Laughton et al., 1970), and the Reykjanes (Figure 4;
116 Vine, 1966), Mohs (Figure 5; Talwani and Eldholm, 1977), and Knipovich (Figure 5; Vogt
117 et al., 1979; Okino et al., 2002) ridges in the North Atlantic Ocean. These five ridges have
118 been surveyed together with the Carlsberg Ridge in the northwest Indian Ocean (Figure 3;
119 Schmidt, 1932; Vine and Matthews, 1963), which is generally considered as a type example
120 of orthogonal-spreading ridge.

121 We have selected in the Harvard centroid moment tensor (CMT) catalog all focal
122 mechanisms of earthquakes shallower than 50 km which occurred between 1976 and 2000 (25
123 years) along these six ridges (Dziewonski et al., 1981). 271 mechanisms of extensional or
124 strike-slip type have been obtained and are plotted in Figures 2 to 5. For each ridge or ridge
125 segment, we determined its mean trend, the mean spreading direction, and the mean stretching
126 direction (Table 1). If necessary, the ridges have been divided in roughly rectilinear segments.
127 For example, the SWIR has been divided into two parts: the northeastern part strikes N54°E
128 on average and the southwestern part N105°E (Figure 2). The ridge mean trend has been
129 directly measured on bathymetric and seismic maps. The mean spreading direction
130 corresponds to the average of the spreading directions calculated at the ridge segment
131 extremities from the NUVEL-1A plate motion model (DeMets et al., 1990; 1994), except for
132 Sheba and Carlsberg ridges for which we used Fournier et al. (2001b) solution (Table 1). The
133 mean stretching direction is computed from the normal faulting solutions (inserts in Figures 2
134 to 5). From these data, the spreading and stretching obliquities have been calculated for each

135 ridge (Table 1). Strike-slip focal mechanisms along transform faults are also plotted in
136 Figures 2 to 5 to show the consistency between slip vectors of strike-slip mechanisms and
137 spreading directions provided by plate motion models.

138 The stretching obliquity (S_{obl}) is plotted against spreading (or rifting) obliquity (R_{obl}) for
139 the selected ridges in Figure 6. Spreading obliquities greater than 45° are never observed
140 along slow-spreading ridges. The points plot along the $S_{obl} = R_{obl} / 2$ line for spreading
141 obliquities less than 30° (Carlsberg, southwestern SWIR, Reykjanes, and Knipovich ridges),
142 and slightly depart from this line for obliquities between 30° and 45° (Mohns, northeastern
143 SWIR, and Sheba ridges).

144

145 **4. Analytical model of oblique rifting**

146 A horizontal plane-strain model of oblique rifting is presented in Figure 6a. A unit
147 length of lithosphere (initial rift) is obliquely extended to a length β measured perpendicularly
148 to the rift axis. β thus defines a stretching factor corresponding to the ratio of the final versus
149 initial length (e.g., McKenzie, 1978). The stretching obliquity, defined as the angle between
150 the normal to the rift trend and greatest principal strain axis of the strain ellipse (ϵ_1), is
151 calculated as a function of the rifting obliquity and β .

152 The finite strain ellipse is calculated from continuum mechanics by decomposing the
153 deformation matrix (deformation gradient tensor) in finite strain (shape and orientation of the
154 strain ellipse in 2D) and finite rotation of the principal strain axes (e.g., Elliot, 1972; Jaeger
155 and Cook, 1979; McKenzie and Jackson, 1983; Fournier et al., 2004b). The eigenvalues and
156 eigenvectors of the finite strain matrix provide the length and orientation of the principal axes
157 of the finite strain ellipse. Exactly the same result is obtained by factorization of the
158 deformation matrix into pure shear and simple shear components (e.g., Sanderson and
159 Marchini, 1986; Tikoff and Fossen, 1993; Fossen and Tikoff, 1993; Tikoff and Teyssier,
160 1994; Krantz, 1995; Fossen and Tikoff, 1998).

161 The strain ellipse resulting from oblique rifting is shown as a function of the rifting
162 obliquity for various values of stretching factor β in Figure 6b. For a given rifting obliquity,

163 the principal strain axes progressively rotate as β increases. For a rifting obliquity of 45° , the
 164 stretching obliquity increases from 24° for $\beta = 1.1$ to 36° for $\beta = 3$. Furthermore, for a
 165 given β , the stretching obliquity increases as the rifting obliquity increases. For example, for
 166 $\beta = 2$, the stretching obliquity increases to 10° to 20° , 32° , 45° , and 63° for rifting obliquity
 167 of 15° to 30° , 45° , 60° , and 75° , respectively.

168 In Figure 6c, the stretching obliquity is plotted against rifting obliquity for various
 169 values of β . When β is small ($\beta < 1.1$), the stretching obliquity is equal to the half of the
 170 rifting obliquity ($S_{obl} = R_{obl} / 2$). With increasing strain ($\beta > 5$), the stretching obliquity
 171 becomes almost equal to the rifting obliquity ($S_{obl} = R_{obl}$).

172

173 5. Discussion

174 These predictions can be compared with the results obtained for the selected oblique-
 175 spreading ridges (Figure 6). For most ridges, the ε_1 direction ranges along the $S_{obl} = R_{obl} / 2$
 176 line, which corresponds to a low amount of extension in the model. A simple interpretation is
 177 that rocks of the Earth's upper crust undergo small strains of a few per cent before brittle
 178 failure occurs and relieves the accumulated strain. The principal strain directions deduced
 179 from earthquake focal mechanisms thus represent the infinitesimal (or instantaneous) strain
 180 ellipsoid.

181 Our results can also be compared with those of Taylor et al. (1994) and Tuckwell et al.
 182 (1996) for the Reykjanes, Mohns, Southwest Indian (NE), and Sheba ridges, provided one
 183 converts their α and ϕ angles into rifting and stretching obliquities:

$$184 \quad \begin{aligned} R_{obl} &= 90 - \alpha \\ S_{obl} &= \phi - \alpha \end{aligned}$$

185 In contrast with us, Taylor et al. (1994) and Tuckwell et al. (1996) defined the stretching
 186 direction as the perpendicular to the mean trend of normal faults in extension zones.

187 We find a very good agreement for the Reykjanes Ridge, where our estimates of
 188 spreading and stretching obliquities differ only by 1° and 4° , respectively, which is smaller
 189 than the uncertainties. For the Mohns Ridge, our results compare well with those of Taylor et

190 al. (1994) but slightly differ from Tuckwell et al. (1996) estimates of spreading obliquity
 191 ($34\pm 8^\circ$ vs $40\pm 6^\circ$), mainly because we (and Taylor et al., 1994) use a different azimuth of
 192 spreading (N119°E vs N110°E). Despite this, we find no large discrepancies between our
 193 estimates of stretching obliquity and theirs. Much larger differences are found for the
 194 Southwest Indian and Sheba ridges: for the former, whereas Taylor et al. (1994) and Tuckwell
 195 et al. (1996) give comparable values of 14° and $23\text{--}27^\circ$ for stretching and spreading
 196 obliquities, we find $29\pm 7^\circ$ and $42\pm 11^\circ$, respectively. These differences are entirely
 197 attributable to different estimates of ridge trend and spreading directions, due to the fact that
 198 Taylor et al. (1994) and Tuckwell et al. (1996) took into account only a small part of the
 199 SWIR located near the Rodrigues triple junction (26°N ; Mitchell, 1991), whereas we have
 200 taken into account all the northeastern part of the SWIR over several thousands kilometres
 201 (Figure 2). However, here again, the determination of stretching directions from earthquake
 202 focal mechanisms gives results comparable to the analysis of normal fault trends. Concerning
 203 the Gulf of Aden (Sheba Ridge), a difference up to $5\text{--}10^\circ$ exists between our values and those
 204 of Taylor et al. (1994) and Tuckwell et al. (1996). Once again, these differences come from
 205 the selection of different study areas. The results of Taylor et al. (1994) and Tuckwell et al.
 206 (1996) concern the westernmost part of the Sheba Ridge near the Gulf of Tadjura (45°E ;
 207 Tamsett and Searle, 1988), whereas our results encompass the entire ridge from 46°E to 56°E
 208 (Figure 3; Table 1). Hence, the differences between our results and those of Taylor et al.
 209 (1994) and Tuckwell et al. (1996) come from different scales of study. Studying normal fault
 210 strikes at ridge axes requires detailed mapping of fault fabrics. Working with focal
 211 mechanisms from the world seismicity catalogs allows surveying of larger areas.

212 In general, the results of Tuckwell et al. (1996) show that most values of stretching vs
 213 rifting obliquities range along the $S_{obl} = R_{obl} / 2$ line, like in the present study. Surprisingly, the
 214 direction of ϵ_1 deduced from infinitesimal strain (earthquakes) does not differ from the
 215 perpendicular to the normal faults, which are markers of finite strain and can have
 216 accommodated a significant amount of deformation. This result suggests that normal faults
 217 initially form perpendicular to the direction of ϵ_1 of the infinitesimal strain ellipsoid, keep this

218 orientation during ongoing extension, and do not significantly rotate as the strain increases.
219 As oblique slip (characterized by oblique focal mechanisms) is seldom observed, this implies
220 that normal faults at ridge axes only accommodate a small amount of deformation during the
221 time when they are located in the seismically active part of the rift (about 2 Ma for a ridge
222 with a half-spreading rate of 5 mm/yr and a 20 km large axial rift).

223

224 **6. Conclusion**

225 Plate-motion models such as RM2 and NUVEL-1 (Minster and Jordan, 1978; DeMets et
226 al., 1990) did not account for slip vectors of extensional focal mechanisms along oceanic
227 ridges. The first reason was of course that, for extensional mechanisms, it is not possible to
228 determine which of the two nodal planes is the fault plane and which is the actual slip vector.
229 The second reason was that at oblique-spreading ridges, slip vectors are not parallel but
230 oblique to the plate relative motion. Here, we demonstrate that, at slow-spreading oblique
231 ridges, the maximum strain axis determined from earthquake focal mechanisms trends
232 halfway between the direction of spreading and the normal to the ridge. Hence, the kinematics
233 of oblique ridges and rifts can possibly be determined from a set of extensional focal
234 mechanisms, without assumption on the fault plane and the slip vector. This result could be
235 useful in continental rifts where transform faults are not developed and plate kinematics
236 difficult to assess. The comparison with an analytical model of oblique rifting shows that
237 these features correspond to small deformations at ridge axes, which is consistent with the
238 fact that earthquakes represent infinitesimal strains. Furthermore, the analysis of normal faults
239 directions (Taylor et al., 1994; Tuckwell et al., 1996) yields similar conclusions, though
240 normal fault heaves represent thousands of co-seismic slips. Yet, compared to the rift width
241 (~10 to 20 km), the cumulated stretching factor on each fault must remain low.

242

243

244 **Acknowledgments.** We are grateful to the Editor W. Dunne and to D. Sanderson and B.
245 Tikoff for their constructive reviews of the manuscript. We thank E. Coudret for valuable

246 discussions at the initiation of this work. Figures were drafted using GMT software (Wessel
247 and Smith, 1991).

248 **References**

- 249 Abelson, M., Agnon, A., 1997. Mechanics of oblique spreading and ridge segmentation.
250 Earth Planetary Science Letter 148, 405-421.
- 251 Acocella, V., Korme, T., 2002. Holocene extension direction along the Main Ethiopian Rift,
252 East Africa. Terra Nova 14, 191-197.
- 253 Appelgate, B., Shor, A. N., 1994. The northern Mid-Atlantic and Reykjanes Ridges:
254 Spreading center morphology between 55°50'N and 63°00'N. Journal of Geophysical
255 Research 99, 17,935-17,956.
- 256 Bonini, M., Souriot, T., Boccaletti, M., Brun, J.-P., 1997. Successive orthogonal and oblique
257 extension episodes in a rift zone: Laboratory experiments with application to the Ethiopian
258 Rift. Tectonics 16, 347-362.
- 259 Carbotte, S. M., Macdonald, K. C., 1994. Comparison of seafloor tectonic fabric at
260 intermediate, fast, and super fast spreading ridges: Influence of spreading rate, plate
261 motions, and ridge segmentation on fault patterns. Journal of Geophysical Research 99,
262 13,609-13,632.
- 263 Clifton, A.E., Schlische, R.W., 2003. Fracture populations on the Reykjanes Peninsula,
264 Iceland: Comparison with experimental clay models of oblique rifting. Journal of
265 Geophysical Research 108, 1-17.
- 266 Clifton, A.E., Schlische, R.W., 2001. Nucleation, growth, and linkage of faults in oblique rift
267 zones: Results from experimental clay models and implications for maximum fault size.
268 Geology 29, 455-458.
- 269 Clifton, A.E., Schlische, R.W., Withjack, M.O., Ackermann, R.V., 2000. Influence of rift
270 obliquity on fault-population systematics: results of experimental clay models. Journal of
271 Structural Geology 22, 1491-1509.
- 272 Dauteuil, O., Brun, J.P., 1996. Deformation partitioning in a slow-spreading ridge
273 undergoing oblique extension (Mohns Ridge, Norwegian Sea). Tectonics 17, 303-310.
- 274 Dauteuil, O., Brun, J.P., 1993. Oblique rifting in a slow-spreading ridge. Nature 361, 145-
275 148.

- 276 Dauteuil, O., Huchon, P., Quemeneur, F., Souriot, T., 2001. Propagation of an oblique
277 spreading centre: the western Gulf of Aden. *Tectonophysics* 332, 423-442.
- 278 DeMets, C., Gordon, R.G., Argus, D.F., Stein, S., 1990. Current plate motion. *Geophysical*
279 *Journal International* 101, 425-478.
- 280 DeMets, C., Gordon, R.G., Argus, D.F., Stein, S., 1994. Effects of recent revisions to the
281 geomagnetic reversal time scale on estimates of current plates motions. *Geophys. Res.*
282 *Lett.* 21, 2191-2194.
- 283 Dewey J.F., Holdsworth, R.E., Strachan, R.A., 1998. Transpression and transtension zones.
284 *In: Holdsworth, R.E., Strachan, R.A. & Dewey, J.F. (eds) Continental Transpressional*
285 *and Transtensional Tectonics*. Geological Society, London, Special Publications 135, 1-
286 14.
- 287 Dziewonski, A. M., Chou, T. A., Woodhouse, J. H., 1981. Determination of earthquake
288 source parameters from waveform data for studies of global and regional seismicity.
289 *Journal of Geophysical Research* 86, 2825-2852.
- 290 Elliott, D., 1972. Deformation paths in structural geology. *Geol. Soc. America Bull.* 83, 2621-
291 2638.
- 292 Engdahl, E.R., van der Hilst, R., Buland, R., 1998. Global teleseismic earthquake relocation
293 with improved travel times and procedures for depth determination. *Bulletin of the*
294 *Seismological Society of America* 88, 722-743.
- 295 Ewing, M., Heezen, B. C., 1960. Continuity of mid-oceanic ridge and rift valley in the
296 southwestern Indian Ocean confirmed. *Science*, 131, 1677-1679.
- 297 Fisher, R.L., Sclater, J.G., 1983. Tectonic evolution of the Southwest Indian Ocean since the
298 mid-Cretaceous: plate motions and stability of the pole of Antarctica-Africa for at least 80
299 Myr. *Geophysical Journal of the Royal Astronomical Society* 73, 553-576.
- 300 Fossen, H., Tikoff, B., 1993. The deformation matrix for simultaneous simple shearing, pure
301 shearing and volume change, and its application to transpression-transtension tectonics. *J.*
302 *Struct. Geol.* 3-5, 413-422.

- 303 Fossen, H., Tikoff, B., 1998. Extended models of transpression and transtension, and
304 application to tectonic settings. *In*: Holdsworth, R.E., Strachan, R.A. & Dewey, J.F. (eds)
305 *Continental Transpressional and Transtensional Tectonics*. Geological Society, London,
306 Special Publications 135, 1-14.
- 307 Fournier, M., Bellahsen, N., Fabbri, O., Gunnell, Y., 2004a. Oblique rifting and segmentation
308 of the NE Gulf of Aden passive margin. *Geochemistry Geophysics Geosystems*, 5,
309 Q11005, doi:10.1029/2004GC000731.
- 310 Fournier, M., Fabbri, O., Angelier, J., Cadet, J.P., 2001a. Kinematics and timing of opening
311 of the Okinawa Trough: Insights from regional seismicity and onland deformation in the
312 Ryukyu arc. *Journal of Geophysical Research* 106, 13,751-13768.
- 313 Fournier, M., Jolivet, L., Davy, P., Thomas, J. C., 2004b. Back arc extension and collision: an
314 experimental approach of the tectonics of Asia. *Geophys. J. Int.* 157, 871-889.
- 315 Fournier, M., Patriat, P., Leroy S., 2001b. Reappraisal of the Arabia-India-Somalia triple
316 junction kinematics. *Earth Planetary Science Letter* 184, 103-114.
- 317 Grindlay, N. R., Madsen, J. A., Rommevaux-Jestin, C., Sclater, J., 1998. A different pattern
318 of ridge segmentation and mantle Bouguer gravity anomalies along the ultra-slow
319 spreading Southwest Indian Ridge (15°30'E to 25°E). *Earth Planetary Science Letter* 161,
320 243-253.
- 321 Jaeger, J.C., Cook, N.G.W., 1979. *Fundamentals of rocks mechanism*. Third Edition,
322 Chapman and Hall, London.
- 323 Krantz, R.W., 1995. The transpressional strain model applied to strike-slip, oblique-
324 convergent and oblique-divergent deformation. *J. Struct. Geol.* 17, 1125-1137.
- 325 Laughton, A.S, Whitmarsh, R.B., Jones M.T., 1970. The evolution of the Gulf of Aden.
326 *Philos. Trans. R. Soc. London*, A267. 227-266.
- 327 Marrett, R., Allmendinger, R.W., 1990. Kinematic analysis of fault-slip data. *Journal of*
328 *Structural Geology* 12, 973-986.
- 329 Mart, Y., Dauteuil, O., 2000. Analogue experiments of propagation of oblique rifts.
330 *Tectonophysics* 316, 121-132.

- 331 Matthews, D. H., Williams, C., Laughton, A. S., 1967. Mid-ocean ridge in the mouth of the
332 Gulf of Aden. *Nature*, 215, 1052-1053.
- 333 McAllister, E., Cann, J., Spencer, S., 1995. The evolution of crustal deformation in an
334 oceanic extensional environment. *Journal of Structural Geology* 17, 183-199.
- 335 McClay, K. R., White, M. J., 1995. Analogue modelling of orthogonal and oblique rifting.
336 *Marine and Petroleum. Geology* 12, 137-151.
- 337 McCoss, A.M. 1986. Simple constructions for deformation in transpression/transension
338 zones. *Journal of Structural Geology* 8, 715-718.
- 339 McKenzie, D. P., 1969. The relationship between fault plane solutions for earthquakes and the
340 directions of the principal stresses. *Bull. Seism. Soc. America* 59, 591-601.
- 341 McKenzie, D.P., 1978. Some remarks on the development of sedimentary basins. *Earth*
342 *Planet. Sci. Lett.*, 40, 25-32.
- 343 McKenzie, D. P., Jackson, J., 1983. The relationship between strain rates, crustal thickening,
344 paleomagnetism, finite strain and fault movements within a deforming zone. *Earth*
345 *Planetary Science Letter* 65, 182-202.
- 346 Minster, J.B., Jordan, T.H., 1978. Present-day plate motions. . *Journal of Geophysical*
347 *Research* 83, 5331-5354.
- 348 Mitchell, N.C., 1991. Distributed extension at the Indian Ocean triple junction. *Journal of*
349 *Geophysical Research* 96, 8019-8043.
- 350 Murton, B. J., Parson, L. M., 1993. Segmentation, volcanism and deformation of oblique
351 spreading centres: A quantitative study of the Reykjanes Ridge. *Tectonophysics*, 222, 237-
352 257.
- 353 Okino, K., Curewitz, D., Asada, M., Tamaki, K., Vogt, P., Crane, K., 2002. Segmentation of
354 the Knipovich Ridge implication for focused magmatism and effect of ridge obliquity at an
355 ultraslow spreading system. *Earth Planetary Science Letter* 202, 275-288.
- 356 Patriat, P., 1987. Reconstitution de l'évolution du système de dorsales de l'Océan Indien par
357 les méthodes de la cinématique des plaques, Territoire des Terres Australes et Antarctique
358 Françaises (ed.), 308 p., PhD Thesis, Université de Paris VI, France.

- 359 Petit, C., Déverchère, J., Houdry, F., San'kov, V.A., Melnikova, V. I., Delvaux, D., 1996.
360 Present-day stress field changes along the Baikal rift and tectonic implications. *Tectonics*
361 15, 1171-1191.
- 362 Sanderson, D. J., Marchini, W. R. D., 1984. Transpression. *Journal of Structural Geology* 6,
363 449-458.
- 364 Sandwell, D.T., Smith, W.H.F., 1997. Marine gravity anomaly from Geosat and ERS-1
365 satellite altimetry. *Journal of Geophysical Research* 102, 10039-10054.
- 366 Schmidt, J., 1932. Dana's Tugt Omkring Jorden, 1928-1930. Gyldendal ed., Copenhagen, 269
367 pp.
- 368 Shaw, P.R., Lin, J., 1993. Causes and consequences of variations in faulting style at the Mid-
369 Atlantic ridge. *Journal of Geophysical Research* 98, 21,839-21,851.
- 370 Sibuet, J.C., Hsu, S.-K., Shyu, C.T., Liu, C.S., 1995. Structural and kinematic evolutions of
371 the Okinawa Trough backarc basin. In: *Backarc Basins: Tectonics and Magmatism*, edited
372 by B. Taylor, pp. 343-379, Plenum, New York.
- 373 Talwani, M., Eldholm, O., 1977. Evolution of the Norwegian-Greenland Sea. *Geological*
374 *Society of America Bulletin* 88, 969-999.
- 375 Tamsett, D., Searle, R., 1988. Structure of the Alula-Fartak fracture zone, Gulf of Aden.
376 *Journal of Geophysical Research* 95, 1239-1254.
- 377 Taylor, B., Crook, K., Sinton, J., 1994. Extensional transform zones and oblique spreading
378 centers. *Journal of Geophysical Research* 99, 19,707-19,718.
- 379 Tikoff, B., Fossen, H., 1993. Simultaneous pure and simple shear: the unifying deformation
380 matrix. *Tectonophysics* 217, 267-283.
- 381 Tikoff, B., Teyssier, C., 1994. Strain modeling of displacement-field partitioning in
382 transpression orogens. *Journal of Structural Geology* 16, 1575-1588.
- 383 Tron, V., Brun, J.-P., 1991. Experiments on oblique rifting in brittle-ductile systems.
384 *Tectonophysics* 188, 71-84.
- 385 Tuckwell, G.W., Bull, J.M., Sanderson, D.J., 1996. Models of fracture orientation at oblique
386 spreading centres. *Journal of the Geological Society London* 153, 185-189.

- 387 Tuckwell, G.W., Bull, J.M., Sanderson, D.J., 1998. Numerical models of faulting at oblique
388 spreading centers. *Journal of Geophysical Research* 103, 15474-15482.
- 389 Twiss, R.J., Unruh, J.R., 1998. Analysis of fault slip inversions: Do they constrain stress or
390 strain rates? *J. Geophys. Res.* 103, 12205-12222.
- 391 Venkat-Ramani, M., Tikoff, B., 2002. Physical models of transtensional folding. *Geology* 30,
392 523-526.
- 393 Vine, F. J., 1966. Spreading of the ocean floor; new evidence. *Science* 154, 1405-1415.
- 394 Vine, F. J., Matthews, D. H., 1963. Magnetic anomalies over oceanic ridges. *Nature* 199, 947-
395 949.
- 396 Vogt, P.R., Taylor, P.T., Kovacs, L.C., Johnson, G.L., 1979. Detailed aeromagnetic
397 investigation of the Arctic Basin. *Journal of Geophysical Research* 84, 1071-1089.
- 398 Wessel, P., Smith, W. M. F., 1991. Free software helps map and display data. *Eos Trans.*
399 *AGU*, 72 (41), 441-446.
- 400 Withjack, M. O., Jamison, W.R., 1986. Deformation produced by oblique rifting.
401 *Tectonophysics* 126, 99-124.

Figure captions

Figure 1. Geometrical relationship between the main structural directions at oblique rifts.

404

Figure 2. Bathymetric map (Sandwell and Smith, 1997), shallow seismicity between 1964 and 1995 (focal depth < 50 km; magnitude > 2; Engdahl et al., 1998), and all available earthquake focal mechanisms (Harvard CMT for the period 1976-2000; Dziewonski et al., 1981) for the Southwest Indian Ridge (SWIR). Inserted stereoplots are equal-area projections of the P and T axes of the extensional focal mechanisms and the mean direction of extension (ϵ_1). The SWIR has been divided into two parts with different trends: the northeastern part between the Rodrigues triple junction and the Prince Edward-Marion-Andrew Bain fracture zone (PEMABFZ; Grindlay et al., 1998) trends N054°E \pm 2°, and the southwestern part between PEMABFZ and 53°S, 14°E trends N105°E \pm 2°. Bathymetric contour interval is 1000m. Strike-slip focal mechanisms along fracture zones show the consistency between slip vector azimuths and directions of relative motion (solid arrows) calculated from plate motion models.

417

Figure 3. Same legend as Figure 2 for the Sheba and Carlsberg ridges. OTF is Owen transform faults. Bathymetric contour interval is 500m.

420

Figure 4. Same legend as Figure 2 for the Reykjanes Ridge. Between 55.5°N, 35.5°W and 63.5°N, 24°W, the ridge strikes N037°E \pm 3°. Bathymetric contour interval is 500m.

423

Figure 5. Same legend as Figure 2 for the Mohns and Knipovich ridges (location in Figure 4). The Mohns Ridge strikes N063°E \pm 2° on average between 71°N, 7.5°W and 73.5°N, 8°E. The mean trend of the Knipovich Ridge between 73.7°N, 9°E and 78°N, 8°E is N178°E \pm 2°. Bathymetric contour interval is 200m.

428

429 Figure 6. Stretching obliquity S_{obl} (maximum principal strain ϵ_1) as a function of spreading
430 obliquity R_{obl} in degrees for seven oblique-spreading ridges. Data sources and abbreviations
431 are given in Table 1. See text for additional explanation. Error bars for spreading obliquity
432 represent the sum of the uncertainties in the measurement of the ridge mean trend and in the
433 azimuth of spreading calculated along the ridge. Error bars for stretching obliquity represent
434 the standard deviation of the T-axes azimuth.

435

436 Figure 7. a. Plane-strain analytical model of oblique rifting. See text for additional
437 explanation. b. Strain ellipse for various stretching factors and rifting obliquities. c.
438 Stretching obliquity S_{obl} as a function of rifting obliquity R_{obl} in degrees. The curves are
439 calculated from the analytical model and the straight lines correspond to $S_{obl} = R_{obl}$ and
440 $S_{obl} = R_{obl} / 2$.

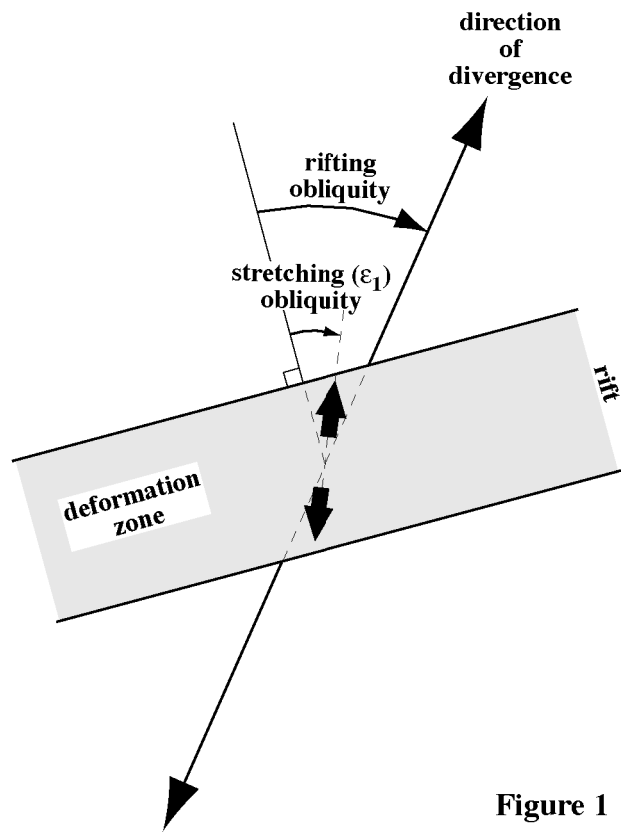


Figure 1

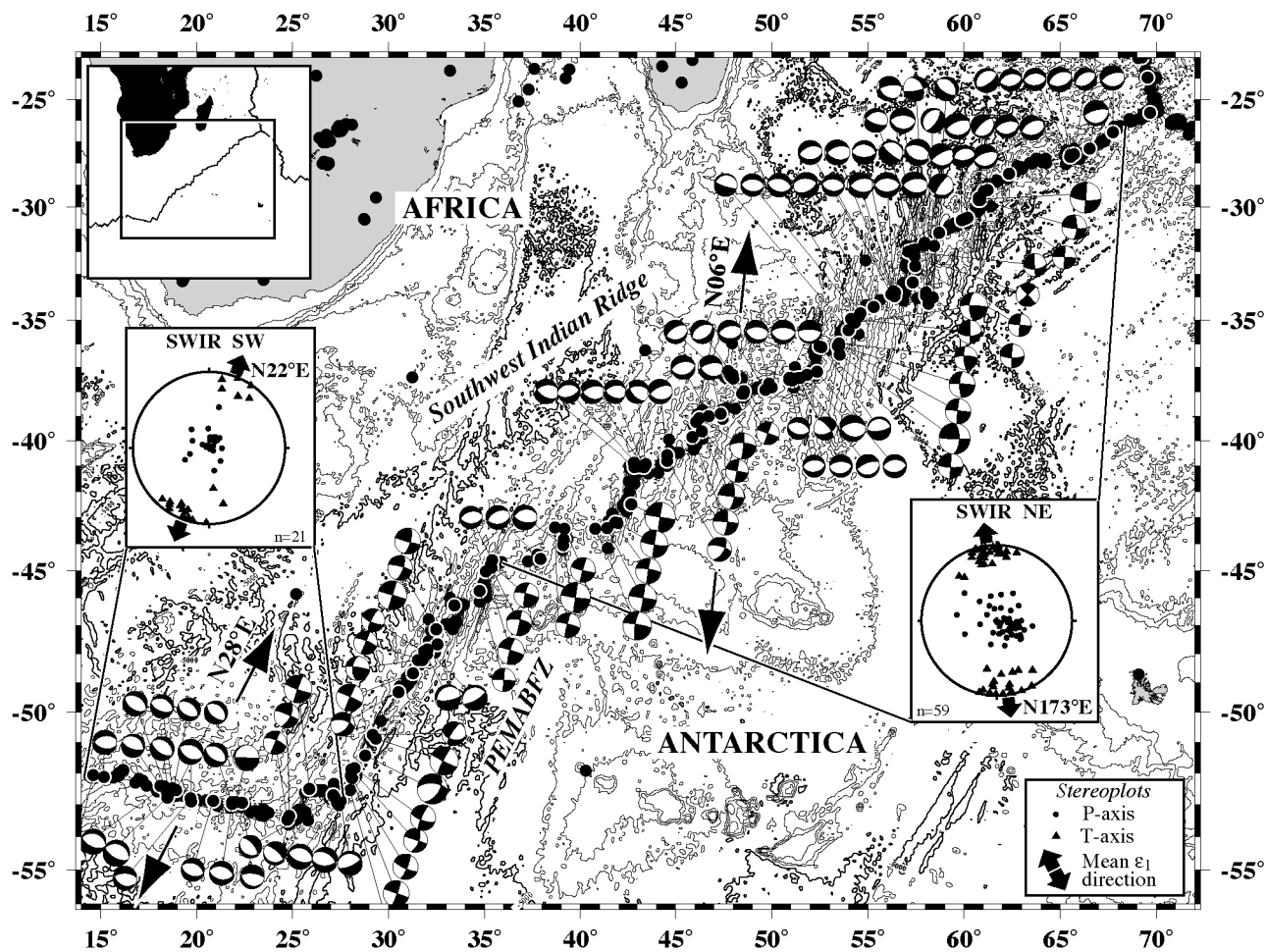


Figure 2

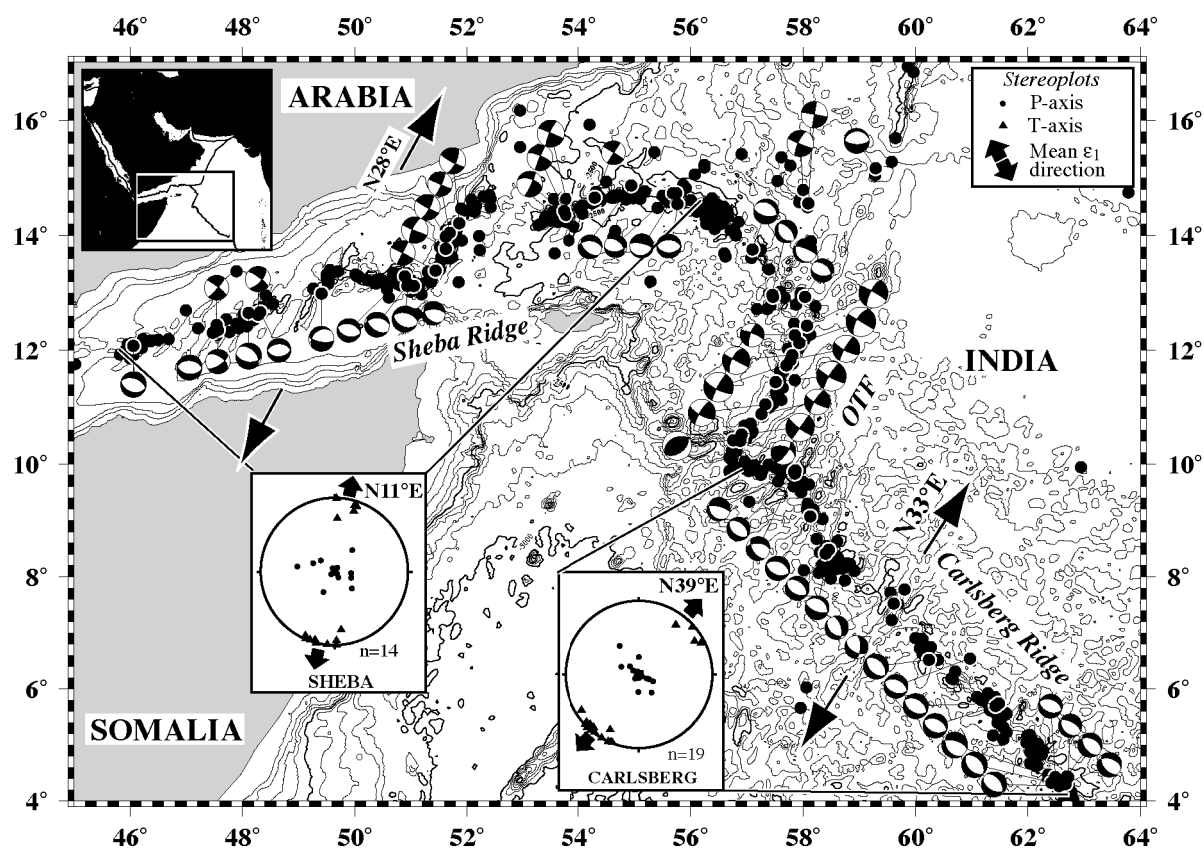


Figure 3

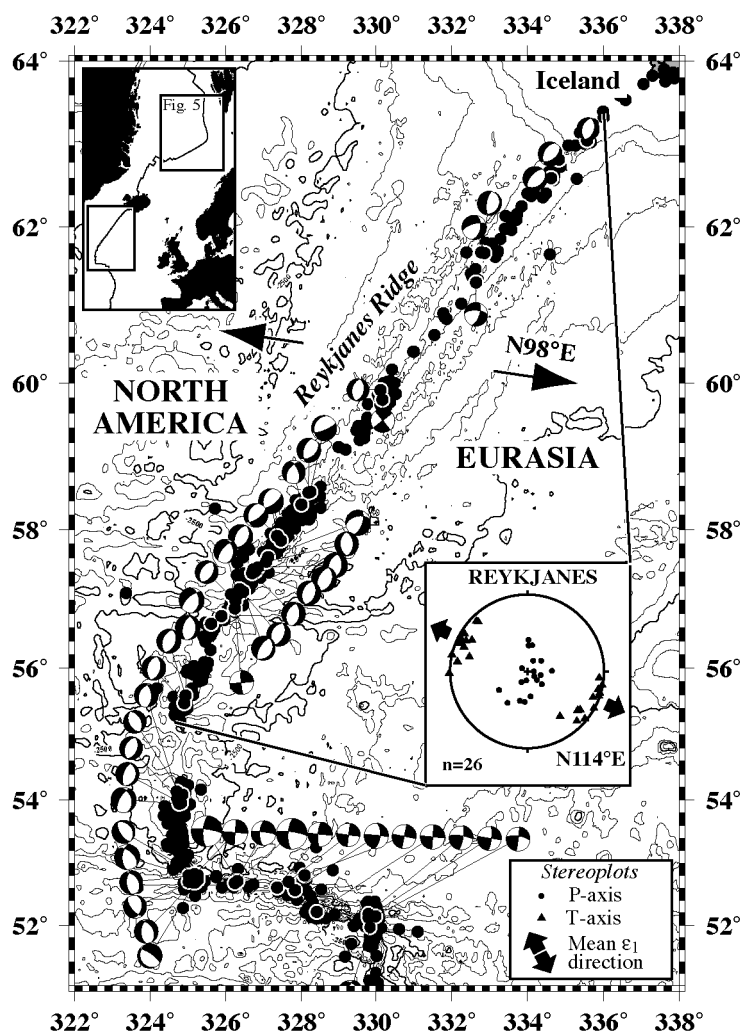


Figure 4

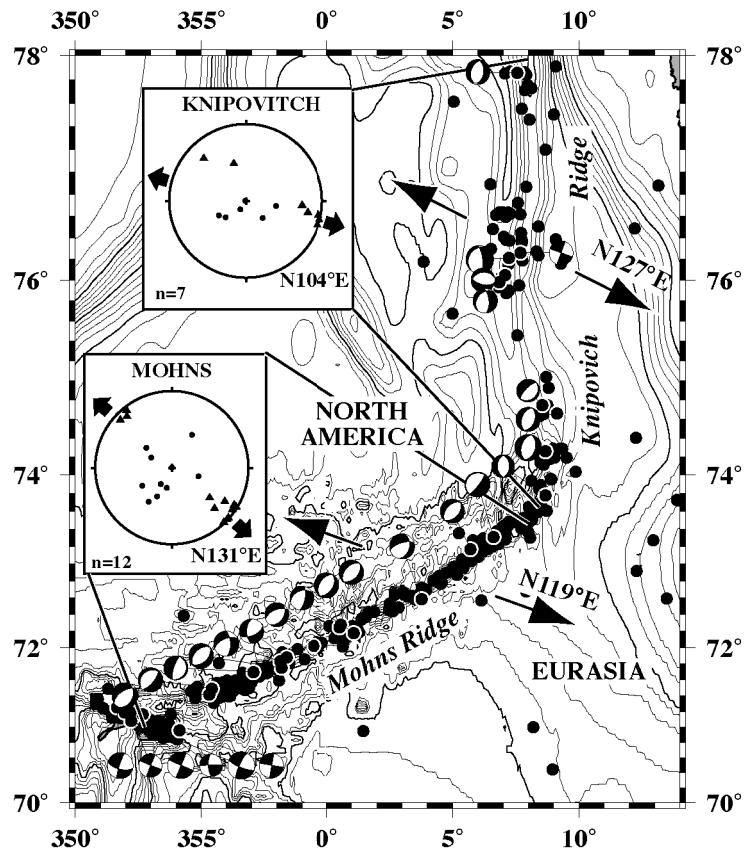


Figure 5

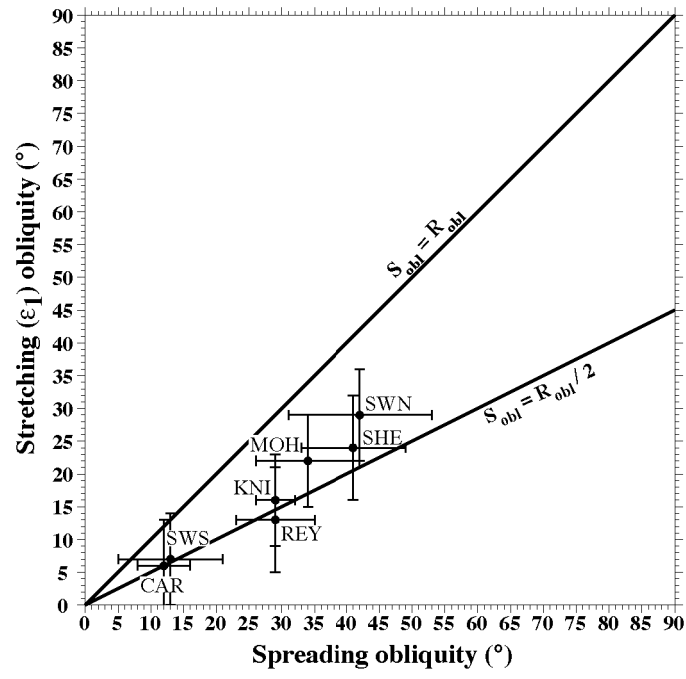


Figure 6

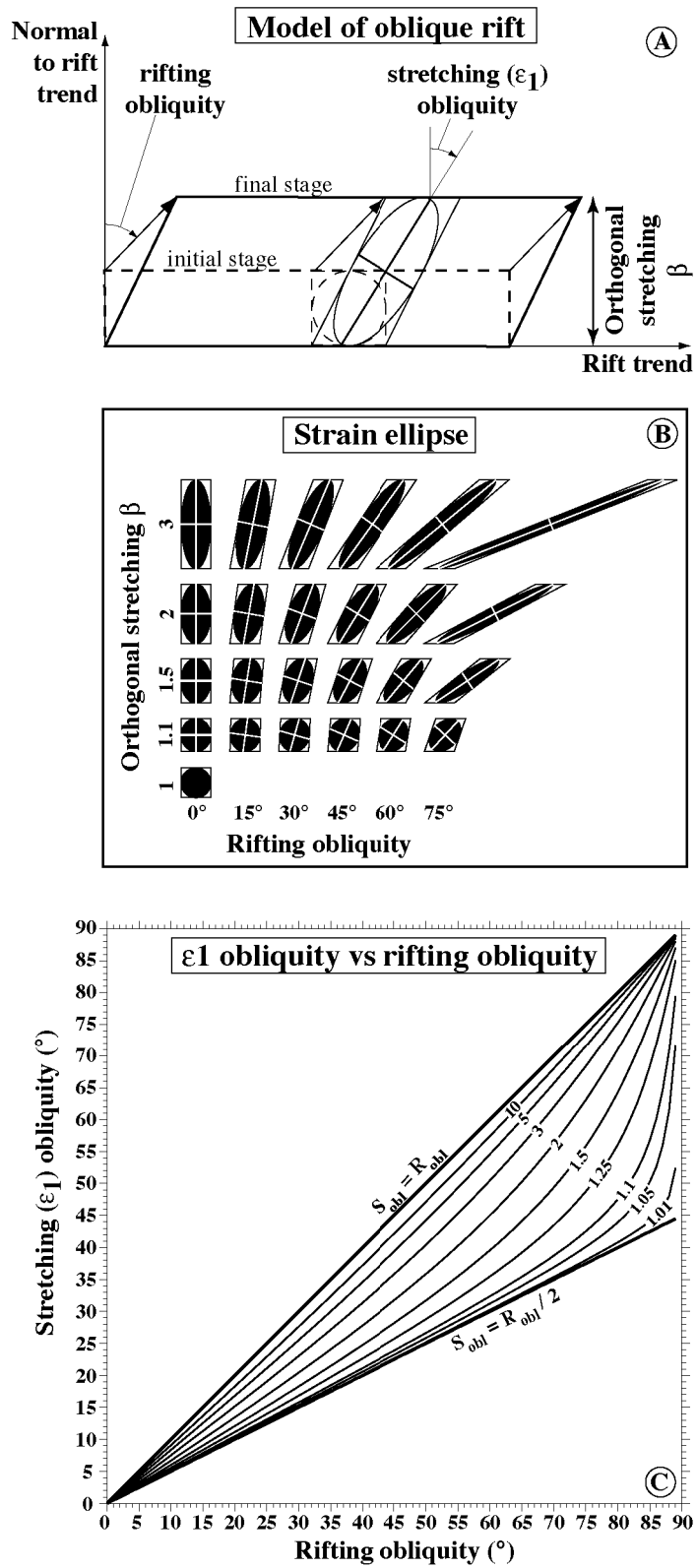


Figure 7

Table 1. Mean trend, azimuth of spreading, spreading obliquity, and principal strain ϵ_1 obliquity for oblique spreading ridges

Ridge	Ridge mean trend (°E)	Ridge extremities			Mean azimuth of spreading (°E)	Mean T-axis Strike, Dip deg	Spreading obliquity deg	Principal strain ϵ_1 obliquity deg	Labels ²
		Latitude (°N)	Longitude (°E)	Azimuth of spreading ¹ (°E)					
Aden - Sheba	N077°E $\pm 3^\circ$	12	46	33	028 ± 5	011, 1 (n=14)	41 ± 8	24 ± 8	SHE
		14.5	56	23					
Carlsberg	N135°E $\pm 2^\circ$	10	57	31	033 ± 2	219, 0 (n=18)	12 ± 4	6 ± 7	CAR
		4	63	35					
SWIR NE	N054°E $\pm 2^\circ$	-45	35	15	006 ± 9	353, 3 (n=59)	42 ± 11	29 ± 7	SWN
		-26	69	177					
SWIR SW	N105°E $\pm 2^\circ$	-52	14	34	028 ± 6	202, 4 (n=21)	13 ± 8	7 ± 7	SWS
		-53	28	22					
Reykjanes	N037°E $\pm 3^\circ$	55.5	-35.5	95	098 ± 3	294, 2 (n=26)	29 ± 6	13 ± 8	REY
		63.5	-24	102					
Mohn	N063°E $\pm 2^\circ$	71	-7.5	113	119 ± 6	131, 4 (n=12)	34 ± 8	22 ± 7	MOH
		73.5	8	125					
Knipovitch	N178°E $\pm 2^\circ$	73.7	9	126	127 ± 1	104, 4 (n=7)	29 ± 3	16 ± 7	KNI
		78	8	128					

n is the number of extensional earthquake focal mechanisms used to determined the mean T-axes azimuth.

¹Azimuths of spreading after DeMets et al. (1990), except for SHE and CAR after Fournier et al. (2001).

²Labels are for data plotted in Figure 5.